Composite left/right-handed stacked hole arrays at sub-millimeter wavelength

Shengxiang Wang, Frédéric Garet, Karine Blary, Charles Croënne, Eric Lheurette, Jean-Louis Coutaz, Didier Lippens

Composite left/right-handed stacked hole arrays at submillimeter wavelengths

Cite as: J. Appl. Phys. **107**, 074510 (2010); https://doi.org/10.1063/1.3374703
Submitted: 08 February 2010 . Accepted: 05 March 2010 . Published Online: 14 April 2010

Shengxiang Wang, Frédéric Garet, Karine Blary, Charles Croënne, Eric Lheurette, Jean-Louis Coutaz, and Didier Lippens

Composite left/right-handed stacked hole arrays at submillimeter wavelengths

Shengxiang Wang,[1] Frédéric Garet,[2] Karine Blary,[1] Charles Croënne,[1] Eric Lheurette,[1] Jean-Louis Coutaz,[2] and Didier Lippens[1,a)]
[1]*Institut d'Electronique de Micro-électronique et de Nanotechnologie, UMR CNRS 8520 Université des Sciences et Technologies de Lille, Avenue Poincaré BP 60069, 59652 Villeneuve d'Ascq Cedex, France*
[2]*Laboratoire IMEP-LAHC, Université de Savoie, 73376 Le Bourget du Lac Cedex, France*

(Received 8 February 2010; accepted 5 March 2010; published online 14 April 2010)

High-transmissivity composite left/right-handed uniaxial bulk metamaterials were fabricated in a multilayered dielectric/hole metal array technology and experimentally assessed at submillimeter wavelengths (0.4–0.9 THz) by time-domain spectroscopy. From the frequency dependence of the complex scattering parameters, we show the possibility to close the gap between the left- and right-handed dispersion branches by increasing the number of layers from 3 to 5. Such a demonstration paves the way of balance composite propagation characteristics with a gapless transition between the negative and positive values of refractive index at a frequency of 0.5 THz.
 [doi:10.1063/1.3374703]

I. INTRODUCTION

The composite electromagnetic characteristic of metamaterial technologies was primarily demonstrated at microwave frequencies for transmission lines loaded by series capacitances and shunt inductances.[1] By a proper engineering of the resonance frequencies of the equivalent series and parallel equivalent circuits, a balance condition was also obtained. In this case, the transition between the ground LH dispersion branch (backward propagation) and the right-handed (RH) one is seamless namely with no forbidden band, where the waves are evanescent. In terms of dispersion characteristics, this means that the group velocity is not vanishing at the wavevector $k=0$, a welcome feature in many applications. Recently, we showed that such a balance composite behavior can also be preserved when ferroelectric varactor elements are integrated within coplanar transmission lines.[2] On the other hand, the composite dispersion concept can be considered for a split ring resonator (SRR)/wire technology.[3] This was notably demonstrated in our group for an omega-type technology where the core of the basic pattern is equivalent to a SRR while the arms play the role of a wire array.[4] Owing to the bulk configuration, it was possible, always at microwave frequencies, to steer the refracted beams at the titled interface of a wedge-type device over the negative-zero-positive angle regions.[5] The demonstration of the balance composite properties at THz frequencies is the next stage of this study, preferably under free space rather than guided wave conditions. Indeed, the latter should allow exploiting the singular refraction properties of metamaterials in the terahertz (THz) frequency band,[6–8] which is unique in terms of potential applications notably for security and environment controls.[9]

The main obstacle to this extension toward THz frequencies is the polarization of the incident magnetic field, which has to be perpendicular to the SRR array. At millimeter waves, the scattering of an impinging wave on a stack of multilayered patterned metal /dielectric substrates with a grazing incidence can be considered.[10] On a similar concept, a LH dispersion branch was therefore demonstrated by using a quartz technology in the 50–75 GHz frequency band.[11] However, further increasing the operating frequency at THz frequency appears very challenging mainly owing to the grazing incidence condition.

A solution to alleviate such an issue is to consider a front-side illumination of subwavelength holes arrays, which mimic current loops along the propagation direction and hence a magnetic response, owing to the contribution of displacement current. At millimeter waves, the pioneering work in this field was performed by the University of Navarra in Spain with several experimental demonstrations around 50 GHz using a drilled aluminum plates technology.[12–14] For these first experimental demonstrations at millimeter wavelengths, the requirement of a subwavelength aperture, as it was the case for observing extraordinary transmission,[15] was early recognized. Several theoretical papers have further formalized the propagation properties of the subwavelength hole arrays, which can be considered as double negative media when they are stacked.[16–18] On these general concepts for fabricating a negative index material under front-side illumination, we recently showed the possibility to further extend the operating frequency in the THz frequency range. To this aim, an experimental demonstration was carried out by showing a phase advance in the propagation of electromagnetic waves through a stack of metal plates with holes arrays spaced by dielectric layers. For this aforementioned work, only the transmission was recorded experimentally and the clue of left-handedness was achieved by retrieving the negative index via the transmission and reflection coefficients which were numerically calculated. In the present paper, we go further in the analysis of the holes array technology operating at THz frequencies by addressing two novel issues with respect to the previous one. The first one is the fact that the complex transmission as well as reflection coefficients

a)Electronic mail: didier.lippens@iemn.univ-lille1.fr.

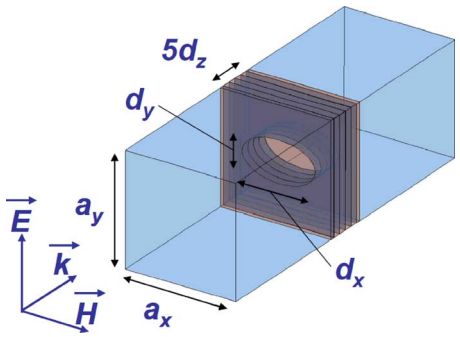

FIG. 1. (Color online) Basic cell stacked along the propagation direction and polarization conditions, $a_x=a_y=340$ μm, $d_x=225$ μm, $d_y=125$ μm, and $d_z=26$ μm.

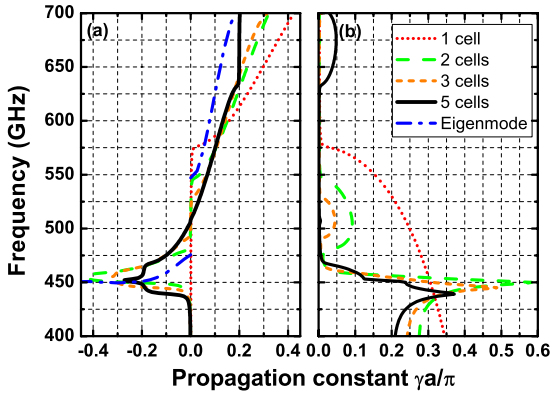

FIG. 2. (Color online) Frequency dependence of (a) the imaginary part β and (b) the real part α of the complex propagation constant as a function of the number of layers varying from 1 to 5. The basic cell dimension along the direction of propagation is a.

were measured experimentally taking benefit of the pump-probe configuration of a time-domain terahertz spectroscopy system. The second one is that several samples were fabricated by varying the number of cells. By this means it was possible to deduce *experimentally* the complex diagram of the propagation constant versus frequency as a function of the number of basic cells. As a key result, it is shown the possibility to induce a *balance* composite dispersion characteristic which is demonstrated for the first time, to our knowledge, at submillimeter frequency range.

The paper is organized as follows: in Sec. II, we analyze some guidelines for the design of a structure operating at THz frequency with main emphasis on the influence of the number of cells. The comparison between the measured and the calculated scattering parameters is reported in Sec. III. At last, the complex propagation constant-frequency diagram is retrieved and discussed in Sec. IV. Concluding remarks and prospects are reported in Sec. V.

II. DESIGN RULES AND DISPERSION CHARACTERISTICS

Figure 1 shows a schematic of the basic cell which consists in an air hole in a metal plate. In the present work, the cells are stacked with dielectric spacer layers along the propagation direction of the electromagnetic wave impinging on the sample under normal incidence. Instead of round-shaped hole arrays which exhibit poor transmission, the hole aperture has been optimized by considering an elliptical aperture.[19,20] A parametric study, by varying the elliptical aspect ratio (EAR), shows that the maximum of transmission is achieved for an EAR of 1.8:1, for an electric field polarization condition along the small axis of the elliptical aperture. It can be shown that the dramatic improvement in the transmissivity results mainly of a resonance in the impedance of the device. By this means impedance matching condition with the surrounding medium can be achieved lowering the reflection losses and thus enhancing the overall transmission. With respect to the operating wavelength, the hole aperture is subwavelength as in an Ebbessen grid where extraordinary transmission can be achieved. Here, this is not the primary reason of a negative index material. As shown below from the study of the dispersion characteristics as a function of the number of layers, the key condition is to stack at least two plates. In addition and in contrast with the thick aluminum plate technology developed at millimeter wave,[14] the metal layer in the present work is made of very thin (0.5 μm thick) gold plated for technology reasons. The spacing dielectric layers are made of low permittivity ($\varepsilon_r \sim 2.6$) dielectric layers.

For the experimental demonstration the operating frequency was chosen around 0.5 THz. This frequency corresponds roughly to the peak power supplied by the THz source of the time-domain spectroscopy (TDS) set up. For this central frequency, the dimensions of the elliptical aperture according to the notation of Fig. 1 are $d_x=225$ μm and $d_y=125$ μm while the basic cell transverse parameters are $a_x=a_y=340$ μm and $a\sim 30$ μm in the propagation direction.

The first stage in the design was to calculate the dispersion characteristic (ω-β), where β is the imaginary part of the complex propagation constant γ, by using the eigenmode solver of the high frequency structure simulator (HFSS) numerical code by ANSOFT. The results of these calculations with the dimensions and material parameters listed above are displayed in Fig. 2(a) in blue dotted-slash lines. A left-handed (LH) dispersion branch from 450 to 475 GHz is noticed for the negative value of β with a positive slope. This means that the group velocity ($v_g=\partial\omega/\partial\beta>0$) and the phase velocity ($v_p=\omega/\beta<0$) are antiparallel, which is the signature of backward propagation. A relatively wide forbidden gap is noticed at higher frequencies from 475 to 550 GHz followed by a conventional RH dispersion branch, plotted here for the positive values of β above 550 GHz.

Let us consider now the dispersion characteristic for a sample with a finite number of layers in the propagation direction. In this case, it is possible to obtain not only the dispersion diagram (ω-β) but also the loss characteristic via the real part (α) of the complex propagation constant. In the present work, the determination of the frequency variations in the complex propagation constant was performed from the frequency dependence of the complex scattering parameters S_{ij} ($i=1,2$) with S_{12} or S_{21} related to the complex transmission coefficients and S_{11} or S_{22} linked to the reflection coefficients. In practice, we used a so-called Fresnel inversion technique,[21] with the following procedure. First, the scatter-

ing matrix is transformed in a chain, also called ABCD, matrix. We then assumed that the propagation takes place in a finite thickness homogeneous sample in which the wave propagation can be depicted by a complex propagation constant $\gamma=\alpha+j\beta$ where α and β describe the evanescence of the waves in the forbidden gap and the propagation in the pass-band, respectively. With this assumption, the ABCD matrix can be expressed as given by equation

$$M=\begin{bmatrix} A & B \\ C & D \end{bmatrix}=\begin{bmatrix} ch(\gamma a) & z\cdot sh(\gamma a) \\ \frac{1}{z}\cdot sh(\gamma a) & ch(\gamma a) \end{bmatrix}, \tag{1}$$

where a is the dimension of the basic cell in the propagation direction and z is the reduced impedance of the propagation medium with respect to its surrounding environment.

By equating term by term the various matrix elements of the structured metamaterial and of the homogeneous media can be shown as

$$\alpha=\frac{1}{a}\ln\left|A\pm\sqrt{A^2-1}\right|, \tag{2}$$

$$\beta a=\angle\left(A\pm\sqrt{A^2-1}\right)+2k\pi, k\in Z. \tag{3}$$

This procedure for retrieving the dispersion characteristics was applied successfully in our group for characterizing the propagation through a photonic crystal slab[22] and to the propagation through a medium constituted of SRR-type metal inclusions.[23] Also, it is worth-mentioning that the complex propagation constant, whose frequency dependence is plotted in Fig. 2, depicts the electromagnetic behavior in the forbidden frequency band and in the pass band. For the former, the real part of γ is thus characteristic of the evanescence of waves with a dramatic decrease in the transmitted wave due to strong reflection. On the contrary for the transmission window, the real part of γ mainly reflects the intrinsic losses owing to a good impedance matching.

For comparing the dispersion characteristics of finite samples to the eigenmode solution, we plotted in Figs. 2(a) and 2(b) the frequency dependence of the imaginary part (β) of the complex propagation constant by taking the number of layers (N) as a parameter The real part (α) versus frequency was plotted in Fig. 2(b).

For $N=1$ (red dotted lines) the dispersion characteristic shows a cutoff frequency around 575 GHz. Below this cutoff, the waves are evanescent within the structures with a nearly parabolic-shaped frequency variation in the attenuation constant α. Above 575 GHz, a RH dispersion branch can be noticed, plotted here up to 700 GHz for a single mode operation. For $N=1$, the main result is thus the *lack* of a LH dispersion branch in the lower frequency part of the investigated spectrum. The electromagnetic behavior of this single plate sample can be compared to the well-known frequency selective surfaces with a high-pass filtering characteristic.[24]

When $N=2$, a LH dispersion branch is apparent for negative values of β which is lying above the eigenmode solution. In this case, the frequency band where the material exhibits a negative index in this case is typically between 460 and 475 GHz. Above this latter frequency this two-cell prototype exhibits a forbidden band followed by a RH dispersion branch above 550 GHz.

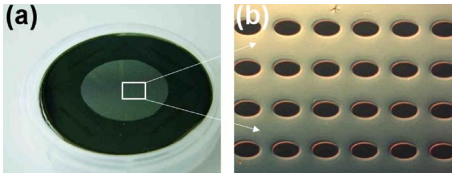

FIG. 3. (Color online) Top photograph of the (a) membranelike structure and (b) an optical microscope zoomed view of aperture hole arrays.

These general trends are similar for the three-cell prototype except the fact that the forbidden band between the LH and RH bands becomes narrower. It results from this behavior as a function of the number of layers that the gap is entirely closed for $N=5$. In Fig. 2, the results for $N=5$ are plotted in black continuous line as a key result. It can be seen that the transition between the LH and RH bands is predicted without a gap in between with a seamless transition between the negative and positive value of the real part of γ. This gap-less transition is also confirmed by the plot of α versus with values close to zero in the vicinity of the corner frequency around 510 GHz while for $N=2$ and $N=3$ a stop-band is pointed out.

III. SCATTERING PARAMETERS: COMPARISON BETWEEN THEORY AND EXPERIMENT

For the experimental verification of the theoretical results outlined above, we fabricated two negative index metamaterial samples with an odd number of layer stacked in the propagation direction. The condition of a negative index precludes $N=1$ since as seen above there is no LH dispersion branch in this case. On this basis $N=3$ and $N=5$ were chosen in order to preserve a reasonable number of layers. Indeed, this is a prerequisite for a successful fabrication of membranelike devices by controlling the increase in the films stress due to stacking.

From a technological point of view, the patterning of the holes in the metal film, deposited by evaporation with a Plassys MEB 550S equipment on a GaAs semi-insulating substrate, was achieved by conventional lift-off photolithography using a Clariant AZnLOF 2070 negative resist [Fig. 3(a)]. The dielectric spacers are benzocyclobutene (BCB) resist layers. BCB, supplied by the Dow Chemical Co., was chosen for its moderate loss (loss tangent ranging from 0.005–0.01 at 1 THz) in the terahertz frequency range, while its permittivity constant given by the supplier is 2.56 at 1 THz. Finally to suppress the substrate effects that introduce an asymmetry in the sample boundaries, interfaced with air on the one side and with a semiconductor on the other side, a membranelike structure was fabricated [Fig. 3(b)]. This was realized by means of a deep backside wet chemical etching ($H_2SO_4:1, H_2O_2:8, H_2O:1$).

The scattering parameter measurements were performed with conventional THz-TDS set ups in a pump-probe configuration. The THz source and detectors, used in both schemes are low temperature grown-GaAs photoswitches,[25]

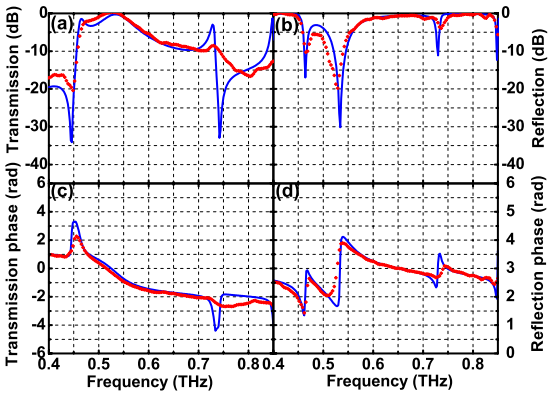

FIG. 4. (Color online) Simulated (solid blue lines) and measured (red symbols) frequency dependence of the magnitude (a) and (b) and of the phase (c) and (d) of the transmission (S_{21}) and reflection (S_{11}) for the three-cells prototype.

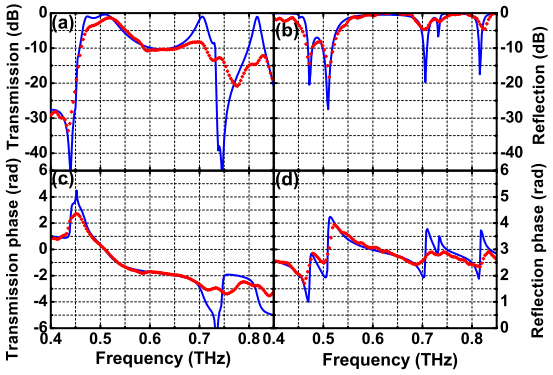

FIG. 5. (Color online) Simulated (solid blue lines) and measured (red symbols) frequency dependence of the magnitude (a) and (b) and of the phase (c) and (d) of the transmission (S_{21}) and reflection (S_{11}) for the three-cells prototype.

which operate under femtosecond laser pulse excitation. The frequency spectrum of the available THz signals, as obtained by a Fourier-transform of the temporal waveforms, ranges from 0.1–5 THz. For the present study focused on the lower part of the submillimeter wave spectrum (0.3–1 THz) the measured dynamics is 60 dB.

For the transmission set up, the THz beam is made almost parallel with a 3 cm waist at 1 THz by means of parabolic mirrors. To avoid spurious effect due to diffraction at the sample edges, we employed a 2 cm diameter diaphragm located in front of the sample, leading to the illumination of about 2700 cells.

In addition, despite the fact that the THz beam delivered by the photoswitch is almost polarized[26] a fine control of the polarization state was realized with grid polarizers, reminding that the electric polarization state corresponds to the electric field directed along the small axis of the elliptical holes. The experimental frequency resolution is 3.75 GHz since temporal waveforms are recorded over a 266 ps time window limited by the maximum delay of the set up.

The specific feature of the reflection set up is mainly the use of a beam splitter which decouples the incident and reflected beams. The THz responses presented below were obtained by differential measurements with and without the sample in the THz beam path. In the case of reflectivity measurements, the reference is given by the signal reflected by a copper mirror.

For a three-cell device, the frequency dependence of the parameter S_{21} was shown in Fig. 4 [magnitude in Fig. 4(a) and phase in Fig. 4(c)]. We also plotted the curves calculated by a full-wave analysis. This comparison was also performed for S_{11} [magnitude in Fig. 4(b) and phase in Fig. 4(d)]. From Fig. 4, it can be noticed the agreement between the calculated and measured data is satisfactory in the lower part of the frequency spectrum, namely between 0.4 and 0.7 THz. As a general comment, it can be seen that the level of transmission in the pass band is high. This is notably true for the LH pass band which is expected to be a ground dispersion band (see Fig. 2) here around 460 GHz. The high level of transmission is a direct consequence of the impedance matching between the device and the free space.

The presence of two pass-bands is notably pointed by the monitoring of the reflection coefficient which shows two dips at 460 GHz and 540 GHz, respectively. In between, around 485 GHz, the reflection coefficient magnitude is high despite the limited number of layer, three in the present case. This is a first clue of the presence of a gap in the vicinity of this frequency.

At higher frequencies, in practice above 700 GHz, the measured data reproduce the features of the transmission spectrum but with a large discrepancy between experimental and calculated data. A numerical analysis of the various propagation modes[27] shows the occurrence of other surface plasmon mode at the frequency where a resonance/antiresonance feature is here observed (~730 GHz). The zero-transmission at 850 GHz can be explained by a Wood anomaly.[28] Indeed, as seen afterwards, this dip in the transmission is not dependent on the number of layers. In addition, the frequency of 860 GHz fits reasonably the Wood anomaly frequency (f_w=882 GHz), which can be calculated from the formula[28] $f_w = c/a_y$ by assuming a scattering of the THz beam with an air /metal interface ($n=1$ and $a_y = 340\ \mu$m).

The analysis of the variations of the phase shows also an excellent agreement in the monomode propagation regime. As a consequence in the following, special attention will be paid to the part of the frequency spectrum below 700 GHz. For the phase of the transmission of the three-cells prototype displayed in Fig. 4(c), the striking result is the increase in the phase shift above the antiresonance at 450 GHz. This is a direct experimental evidence of the LH character of the ground pass-band which will be confirmed in Sec. III by the retrieval of the dispersion characteristics. Basically, the singular electromagnetic (EM) properties of the present propagation involves the transmission through subwavelength hole array and the propagation of surface plasmon in the BCB layer (for further details see Ref. 19). The later phenomenon is resonant in essence with nearly the matching of the longitudinal dimension of the hole (a_y) to the wavelength of the internal surface plasmon mode. Here, we used the same terminology of Ref. 16 where external plasmons at the boundary of the sample are distinguished from the internal ones which propagate within the dielectric spacing layers. This

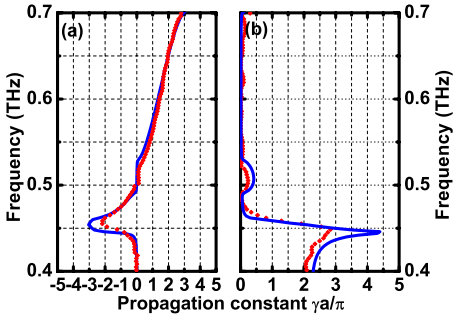

FIG. 6. (Color online) Simulated (solid blue lines) and measured (red symbols) dispersion diagram with the imaginary (a) and real (b) parts of the propagation constant for the three-cells prototype.

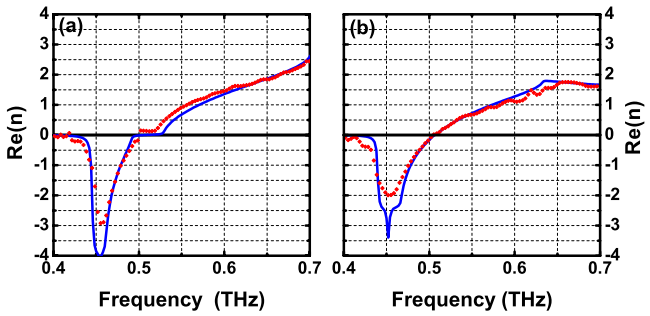

FIG. 8. (Color online) Simulated (solid blue lines) and measured (red symbols) frequency dependence of the real part of the refractive index of the three-cells prototype (a) and five-cells prototype (b).

resonant character is notably pointed out in the frequency dependence of the phase of the reflection coefficient plotted in Fig. 4(d).

The conclusions drawn above apply to the results we measured and calculated for the five-cell sample. However, a main difference can be seen in the transmission window which appears for this case relatively broad. The central frequency of the LH and RH bands can be detected via the magnitude of the reflection coefficient [Fig. 5(b) with two dips at 465 GHz and 510 GHz, respectively. The smoothing in the transition between the two pass-bands indicates that the gap between the two LH and RH dispersion branches is at least narrower with respect to the previous one. The confirmation of the absence of gap, as predicted by the theoretical analysis of Sec. II, requires retrieving now experimentally the dispersion characteristics.

IV. EXPERIMENTAL DISPERSION CHARACTERISTICS

Figure 6 displays the measured and calculated dispersion for a three-cells prototype between 400 and 700 GHz, therefore below the occurrence of a Wood anomaly. The theoretical results are here compared to those which can be retrieved from the scattering parameters measurements. The presence of a gap between the LH and RH dispersion branches is here clearly apparent with a plateau in the dispersion and a bump-shaped variation in the attenuation constant versus frequency which is characteristic of a forbidden band.

Figure 7 shows the comparison which was carried out for the five-cells sample. The key result is the experimental confirmation of a gap-less transition between the LH and RH bands pointed out by a continuity of the first derivative of the ω-β diagram around 500 GHz which corresponds to the center of the Brillouin zone. On the other hand, the absence of gap is also confirmed by the near-zero values of α over a broad frequency spectrum, a welcome feature for many applications.

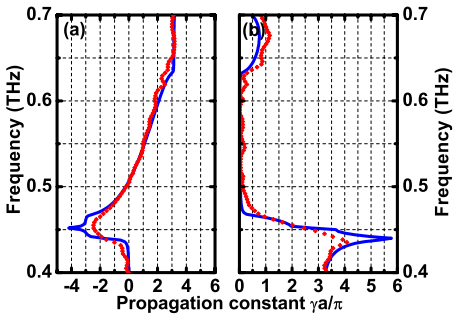

FIG. 7. (Color online) Simulated (solid blue lines) and measured (red symbols) dispersion diagram with the imaginary (a) and real (b) parts of the propagation constant for the five-cells prototype.

Figure 8 shows the frequency dependence of the real part of the effective refractive index calculated and retrieved from the experimental transmission and reflection data for a three-cell and five-cell prototype. The figure confirms the opening of a gap for a three-cell device while a seamless transition is achieved between the LH and RH dispersion branches for the five-cell sample.

V. CONCLUSION AND PROSPECTS

In summary, we showed the possibility to close the gap of a front-side illuminated metamaterial structures, made of a metal/dielectric multilayer, operating at submillimeter wavelengths. It results in a *balanced composite* dispersion characteristic which opens the way to fabricate zero-index metamaterials at THz frequencies. In addition, it was shown that a highly transparent LH window can be fabricated at THz frequency mainly by solving the problem of impedance matching. The solution used here was to implement hole arrays with elliptical apertures and thus sensitive to the field polarization. However, it is believed that this polarization dependence can be overcome with cross-shaped hole structures as already demonstrated for frequency selective surfaces.

ACKNOWLEDGMENTS

This project was carried out in the framework of a collaboration between the University of Lille and the University of Savoie with the technological work carried within the French technological facility network (RENATECH). The authors would like also thank J. Carbonell from the University of Valencia (Spain) for helpful discussions.

[1]C. Caloz and T. Itoh, *Electromagnetic Metamaterials: Transmission Line Theory and Microwave Application* (Wiley, New Jersey, 2006), p. 59.
[2]A. Marteau, G. Vélu, G. Houzet, L. Burgnies, E. Lheurette, J. C. Carru, and D. Lippens, Appl. Phys. Lett. **94**, 023507 (2009).
[3]R. Marqués, F. Martin, and M. Sorolla, *Metamaterials with Negative Parameters: Theory, Design, and Microwave Applications* (Wiley, New Jersey, 2008).

[4]F. Zhang, G. Houzet, E. Lheurette, D. Lippens, M. Chaubet, and X. Zhao, J. Appl. Phys. **103**, 084312 (2008).
[5]F. Zhang, S. Potet, J. Carbonell, E. Lheurette, O. Vanbesien, X. Zhao, and D. Lippens, IEEE Trans. Microwave Theory Tech. **56**, 2566 (2008).
[6]C. M. Bingham, H. Tao, X. Liu, R. D. Averitt, X. Zhang, and W. J. Padilla, Opt. Express **16**, 18565 (2008).
[7]H.-T. Chen, J. F. O'Hara, A. K. Azad, A. J. Taylor, R. D. Averitt, D. B. Shrekenhamer, and W. J. Padilla, Nat. Photonics **2**, 295 (2008).
[8]R. Singh, E. Plum, C. Menzel, C. Rockstuhl, A. K. Azad, R. A. Cheville, F. Lederer, W. Zhang, and N. I. Zheludev, Phys. Rev. B **80**, 153104 (2009).
[9]Z. Jakšić, O. Jakšić, Z. Djurić, and C. Kment, J. Opt. A, Pure Appl. Opt. **9**, S377 (2007).
[10]M. Gokkavas, K. Guven, I. Bulu, K. Aydin, R. S. Penciu, M. Kafesaki, C. M. Soukoulis, and E. Ozbay, Phys. Rev. B **73**, 193103 (2006).
[11]F. Zhang, D. P. Gaillot, C. Croënne, E. Lheurette, X. Melique, and D. Lippens, Appl. Phys. Lett. **93**, 083104 (2008).
[12]M. Beruete, M. Navarro-Cia, M. Sorolla, and I. Campillo, Phys. Rev. B **79**, 195107 (2009).
[13]M. Navarro-Cia, M. Beruete, M. Sorolla, and I. Campillo, Opt. Express **16**, 560 (2008).
[14]M. Beruete, M. Sorolla, and I. Campillo, Opt. Express **14**, 5445 (2006).
[15]T. W. Ebbesen, H. J. Lezec, H. F. Ghaemi, T. Thio, and P. A. Wolff, Nature (London) **391**, 667 (1998).
[16]R. Ortuño, C. Garcia-Meca, F. J. Rodriguez-Fortuno, J. Marti, and M. Alejandro, Phys. Rev. B **79**, 075425 (2009).
[17]A. Mary, S. G. Rodrigo, F. J. Garcia-Vidal, and L. Martin-Moreno, Phys. Rev. Lett. **101**, 103902 (2008).
[18]A. Mary, S. G. Rodrigo, L. Martín-Moreno, and F. J. García-Vidal, Phys. Rev. B **80**, 165431 (2009).
[19]C. Croënne, F. Garet, E. Lheurette, J.-L. Coutaz, and D. Lippens, Appl. Phys. Lett. **94**, 133112 (2009).
[20]C. Croënne, F. Garet, J. Carbonell, E. Lheurette, K. Blary, J. L. Coutaz, and D. Lippens, Proceedings of 39th European Microwave Conference, 2009, p. 626.
[21]D. R. Smith, S. Schultz, P. Markos, and C. M. Soukoulis, Phys. Rev. B **65**, 195104 (2002).
[22]C. Croënne, N. Fabre, D. P. Gaillot, O. Vanbésien, and D. Lippens, Phys. Rev. B **77**, 125333 (2008).
[23]C. Croënne, M. F. Foulon, É. Lheurette, X. Mélique, M. Gheudin, and D. Lippens, Proceedings of European Microwave Association, 2008, Vol. 4, p. 95.
[24]F. Medina, F. Mesa, and R. Marques, IEEE Trans. Microwave Theory Tech. **56**, 3108 (2008).
[25]F. Aquistapace, L. Duvillaret, F. Garet, J. F. Roux, and J. L. Coutaz, J. Appl. Phys. **94**, 7888 (2003).
[26]F. Garet, L. Duvillaret, and J.-L. Coutaz, Proc. SPIE **3617**, 30 (1999).
[27]J. Carbonell, C. Croënne, F. Garet, É. Lheurette, J.-L. Coutaz, and D. Lippens, Proceedings of Metamaterials, London, 30th August–4th September 2009.
[28]R. W. Wood, Phys. Rev. **48**, 928 (1935).